Conformational Events during Ternary Enzyme−Substrate Complex Formation Are Rate Limiting in the Catalytic Cycle of the Light-Driven Enzyme Protochlorophyllide Oxidoreductase[†]

Derren J. Heyes,* Binuraj R. K. Menon, Michiyo Sakuma, and Nigel S. Scrutton*

Manchester Interdisciplinary Biocentre, Faculty of Life Sciences, University of Manchester, 131 Princess Street, Manchester M1 7DN, U.K.

Received August 12, 2008; Revised Manuscript Received August 22, 2008

ABSTRACT: The light-driven enzyme, protochlorophyllide oxidoreductase (POR), has proven to be an excellent model system for studying the role of protein motions during catalysis. POR catalyzes the *trans* addition of hydrogen across the C17−C18 double bond of protochlorophyllide (Pchlide), which is a key step in chlorophyll biosynthesis. While we currently have a detailed understanding of the initial photochemical events and the subsequent hydrogen transfer reactions, there remains a lack of information about the slower substrate binding events leading to the formation of the catalytically active ternary complex. As POR is light-activated, it is relatively straightforward to isolate the ternary enzyme−substrate complex in the dark prior to catalysis, which has facilitated the use of a variety of spectroscopic and kinetic probes to study the binding of both substrates. Herein, we provide a detailed kinetic and thermodynamic description of these processes and show that the binding events are complex, involving multiple conformational states en route to the formation of a ternary complex that is primed for photoactivation. The initial binding of NADPH involves three distinct steps, which appear to be necessary for the optimal alignment of the cofactor in the enzyme active site. This is followed by the binding of the Pchlide substrate and subsequent substrate-induced conformational changes within the enzyme that occur prior to the formation of the final "poised" conformational state. These studies, which provide important information on the formation of the reactive conformation, reveal that ternary complex formation is the rate-limiting step in the overall reaction and is controlled by slow conformational changes in the protein.

Protochlorophyllide oxidoreductase (POR;[1] EC 1.3.1.33) is a light-activated enzyme that has proven to be an excellent model system for studying the role of protein dynamics and thermodynamics in enzyme catalysis (*1*). POR catalyzes the light-dependent *trans* addition of hydrogen across the C17−C18 double bond of the *D*-ring of protochlorophyllide (Pchlide) to produce chlorophyllide (Chlide) (Figure 1), which is a key reaction within the chlorophyll biosynthesis pathway and the subsequent assembly of the photosynthetic apparatus (*1*−*3*). In addition, POR has previously been shown to be a member of the large short-chain dehydrogenase/reductase (SDR) superfamily, which includes other well-studied enzymes such as carbonyl reductase, alcohol dehydrogenase and dihydrofolate reductase (*4*−*7*). However, the experimental advantages offered by studying a light-activated enzyme make POR an important model system for elucidating the mechanism of catalysis by this family of enzymes, and more generally, for enzyme catalysis involving proton and hydride transfers.

During the reaction a hydride is transferred from the *pro-S* face of the nicotinamide ring of NADPH to the C17 position of the Pchlide molecule (*8, 9*) and a conserved Tyr residue has been proposed to donate a proton to the C18 position (*10*). The close proximity of a conserved Lys residue is thought to allow the deprotonation to occur at physiological pH by lowering the apparent pK_a of the phenolic group of the Tyr (*10*). As POR is driven by light, the ternary enzyme: substrate complex can be formed in the dark, prior to catalysis, thus removing the diffusive components from the kinetic analyses. The reaction can then be initiated by illumination at low temperatures, which allows intermediates in the catalytic cycle to be trapped and characterized using a range of spectroscopic techniques (*11*−*16*). Consequently, a number of catalytic steps, involving the initial photochemistry followed by a series of "dark" reactions, have been identified, resulting in a comprehensive understanding of the entire reaction pathway (*13*−*15*). The initial light-driven step, which can occur below 200 K, results in the formation of a nonfluorescent intermediate with a broad absorbance band at 696 nm (*13*). Subsequent EPR, ENDOR and Stark studies, in conjunction with low temperature absorbance spectroscopy, revealed that this intermediate is a charge-transfer complex that is formed by hydride transfer from the NADPH

[†] This work was supported by the UK Biotechnology and Biological Sciences Research Council, UK. N.S.S. is a BBSRC Professorial Fellow.

* Correspondence should be addressed to either. D.J.H. or N.S.S., Manchester Interdisciplinary Biocentre, Faculty of Life Sciences, University of Manchester, 131 Princess Street, Manchester M1 7DN, U.K. Tel: +44 (0)161 3065159. Fax: +44 (0)161 3065201. E-mail: derren.heyes@manchester.ac.uk; nigel.scrutton@manchester.ac.uk.

[1] Abbreviations: Pchlide, protochlorophyllide; Chlide, chlorophyllide; POR, NADPH:protochlorophyllide oxidoreductase; SDR, short-chain dehydrogenase/reductase.

10.1021/bi801521c CCC: $40.75
Published on Web 09/18/2008

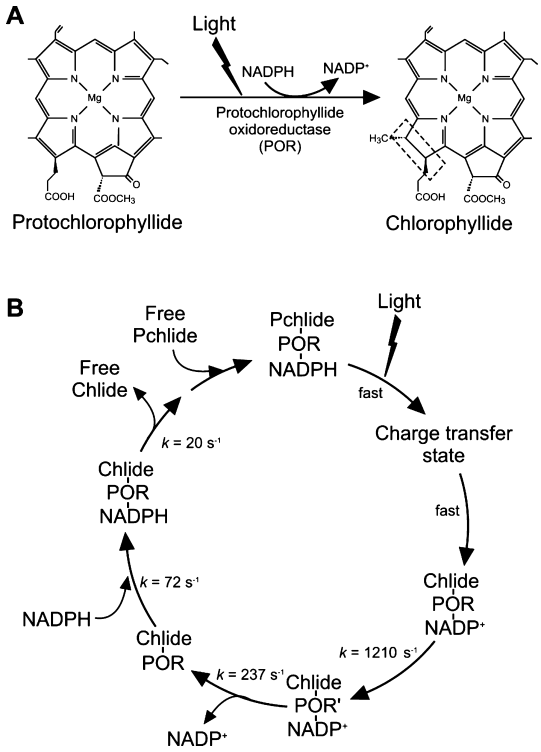

FIGURE 1: The light-driven reduction of protochlorophyllide (Pchlide). (A) The *trans* addition of hydrogen across the C17−C18 double bond of Pchlide to form chlorophyllide (Chlide) in the chlorophyll biosynthesis pathway is catalyzed by the light-driven enzyme, protochlorophyllide oxidoreductase (POR). (B) An overall scheme for the catalytic cycle of POR showing the stepwise formation of the reaction intermediates together with the rate constants that have been calculated previously (*17*).

molecule to the C17 position of Pchlide (*16*). This then facilitates the protonation of the C18 position of Pchlide from the protein during the first of the "dark" reactions (*16*).

A role for domain movements and/or reorganization of the protein has been proposed for the remaining "dark" steps in the reaction, which only occur close to, or above, the "glass transition" temperature of proteins (*14, 15*). These latter catalytic events have been shown to represent a series of ordered product release and cofactor binding events. First, $NADP^+$ is released from the enzyme and is replaced by the NADPH coenzyme. This is followed by release of the Chlide product and subsequent binding of the Pchlide substrate to complete the catalytic cycle (*15*). Laser photoexcitation techniques have also been used to follow the interconversion of the various bound/unbound Chlide product species, which has provided a detailed thermodynamic and kinetic description of these latter steps in the catalytic cycle (*17*).

In addition to using cryogenic temperatures to identify catalytic intermediates it is also possible to study the reaction by using ultrafast pulses of light (*18*−*22*). These measurements have revealed that spectral changes on the picosecond time scale are likely to represent conformational changes that occur before the reduction of Pchlide (*21, 22*). Furthermore, it appears that prior excitation with a laser pulse leads to a more efficient conformation of the active site and an enhancement in the catalytic efficiency of the enzyme (*22*). While all of these studies have provided a detailed understanding of the chemistry and product release steps in the catalytic cycle, little is currently known about the rate-limiting steps in the overall catalytic cycle, which are likely to involve substrate binding and any associated conformational changes. In contrast to the majority of enzyme systems, with POR it is possible to isolate the ternary enzyme−substrate species in the dark, thus removing any subsequent catalytic events that proceed upon illumination from the kinetic analyses. Consequently, in the present work we have been able to measure the kinetics and thermodynamics of binding of both substrates and identified a series of conformational changes using a range of spectroscopic techniques in conjunction with stopped-flow methods. Our studies reveal that the binding processes are complex with multiple steps required to form the active ternary enzyme substrate complex. In addition, we show that ternary complex formation is the rate-limiting step in the overall reaction cycle and is controlled by slow conformational changes in the protein.

MATERIALS AND METHODS

Sample Preparation. All chemicals were obtained from Sigma-Aldrich, except NADPH and $NADP^+$ (Melford Laboratories). Recombinant POR from the thermophilic cyanobacteria *Thermosynechococcus elongatus* was overexpressed in *Escherichia coli* and purified as previously described (*15*). The Pchlide pigment was produced and purified as previously described (*15*).

Absorbance and Fluorescence Measurements. Absorbance measurements were recorded using a Cary 300 UV/visible spectrophotometer (Varian Inc.) in 50 mM Tris pH 7.5, 0.1% (v/v) 2-mercaptoethanol, 0.1% (v/v) Genapol X-080. Fluorescence emission and anisotropy measurements were performed using a QuantaMaster fluorimeter (Photon Technology International) in 50 mM Tris pH 7.5, 0.1% (v/v) 2-mercaptoethanol, 0.1% (v/v) Genapol X-080 at 25 °C. The exciting light was provided from a xenon light source and excitation and emission slit widths were 3 nm.

Stopped-Flow Experiments. Stopped-flow fluorescence and anisotropy kinetics were measured by using a Hi-Tech Scientific SF-61SX2 stopped-flow spectrophotometer (TgK Scientific, Bradford on Avon, U.K.). For fluorescence energy transfer from Trp to NADPH, POR (final reaction cell concentration of 1 μM) in 50 mM Tris pH 7.5, 0.1% (v/v) 2-mercaptoethanol was mixed with various concentrations of NADPH at 25 °C and the fluorescence was measured by using an excitation wavelength of 295 nm and a 400 nm cut-off filter on the emission detector. For fluorescence anisotropy measurements, various concentrations of POR were mixed with either NADPH (final reaction cell concentration of 2 μM) in 50 mM Tris pH 7.5, 0.1% (v/v) 2-mercaptoethanol or Pchlide (final reaction cell concentration of 2 μM) in 50 mM Tris pH 7.5, 0.1% (v/v) 2-mercaptoethanol, 0.1% (v/v) Genapol X-080 at 25 °C. The fluorescence anisotropy of NADPH was measured using an excitation wavelength of 340 nm and a 400 nm cut-off filter on the emission detector, and the fluorescence anisotropy of Pchlide was measured using an excitation wavelength of 450 nm and a 595 nm cut-off filter on the emission detector. The rapid binding of Pchlide was followed by measuring the absorbance at 642 nm using an Applied Photophysics SX.18MV stopped-flow spectrophotometer. Various concentrations of POR in the presence of 2.5 mM $NADP^+$ were mixed with Pchlide (final reaction cell concentration of 2 μM) in 50 mM Tris pH 7.5, 0.1% (v/v) 2-mercaptoethanol,

0.1% (v/v) Genapol X-080 at 25 °C. All measurements were repeated at least 3 times, and transients were analyzed by fitting to a standard single- or double-exponential expression. Where appropriate, the concentration dependence of k_{obs} was analyzed by fitting to eq 1 to obtain values for the apparent dissociation constant for the enzyme−substrate complex, K_d:

$$k_{obs} = k_{max}[S]/(K_d + [S]) \quad (1)$$

where k_{obs} is the observed rate constant at each concentration and k_{max} is the maximum rate constant as [S] approaches infinity. For temperature dependence studies of rate constants, measurements were repeated at various temperatures between 5−50 °C by using a circulating water bath (Fisherbrand) and the thermodynamic parameters were obtained by fitting the data to the Eyring equation.

FTIR Spectroscopy. FTIR spectra were measured using a Vertex 80 spectrometer (Bruker Optics, Ettlingen, Germany). Measurements were recorded in 50 mM Tris pH 7.5, 0.1% (v/v) 2-mercaptoethanol, 0.1% (v/v) Genapol X-080 at 25 °C using an AquaSpec flow cell accessory (MicroBiolytics, Freiburg, Germany) and a buffer only sample as the background. IR absorbance difference signals in the frequency range 1600−1700 cm^{-1} can be assigned to the amide I protein region and changes in the frequency range 1500−1600 cm^{-1} can be assigned to the amide II region.

RESULTS

Binding of NADPH to POR. The binding of NADPH to the enzyme was followed by measuring the FRET signal from Trp residue(s) in the protein to the NADPH coenzyme (Figure 2A). Upon binding there is a quenching of the Trp fluorescence emission band at approximately 320 nm together with a simultaneous increase in the fluorescence emission from NADPH at approximately 450 nm. By measuring the maximum quenching in the Trp fluorescence signal and by assuming a Forster distance for Trp→NADPH energy transfer of 23.4 Å (*23*) the distance from the proposed Trp donor (Trp 31) to the NADPH molecule was calculated to be 21.9 Å. We have been able to measure the rate of NADPH binding by exciting samples at 295 nm and monitoring the increase in NADPH fluorescence following rapid mixing in a stopped-flow spectrometer. The kinetics of NADPH binding were found to be complex and kinetic traces were fitted to three distinct phases (Figure 2B). Subsequently, the observed rate constants for each kinetic phase were measured over a range of NADPH concentrations, and are shown graphically in Figure 2C. Under the pseudo-first-order conditions used in the stopped-flow experiments none of the phases exhibited a dependence on the concentration of NADPH. The rates and relative amplitudes of each phase are shown in Table 1, and the data reveal that the majority of the fluorescence signal comes from the initial step in the binding process.

In addition to using FRET signals, there is also an increase in fluorescence anisotropy from the NADPH molecule upon binding to POR. The fluorescence anisotropy at 435 nm increases from approximately 0.09 in the absence of enzyme to approximately 0.28 at 2 μM POR. This anisotropy change can also be used as a separate probe to measure the rate of NADPH binding in a stopped-flow instrument. Again, the rate of increase in fluorescence anisotropy was shown to follow triphasic kinetics with similar rate constants to those

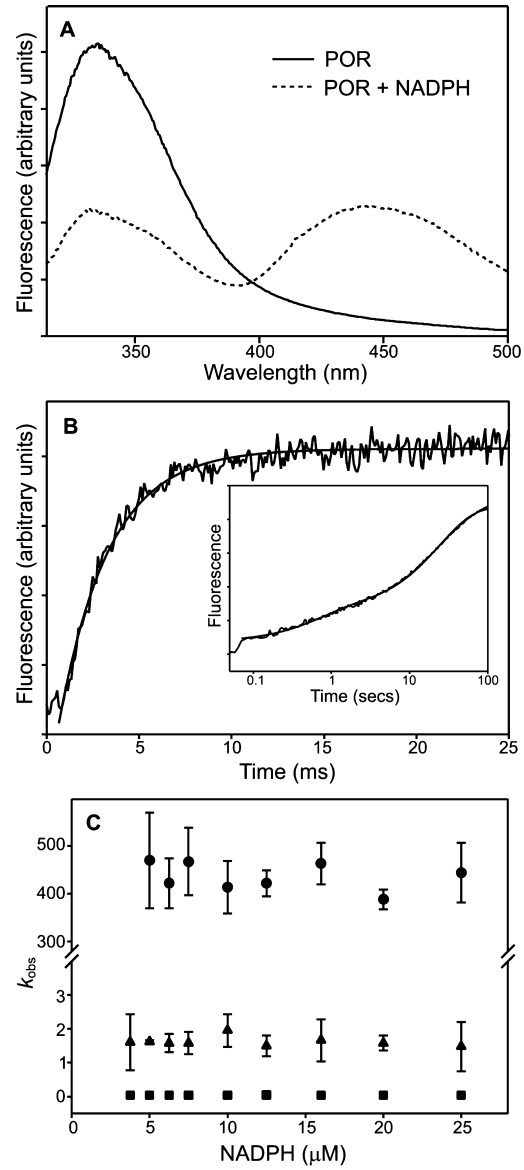

FIGURE 2: The binding of NADPH measured by fluorescence energy transfer. (A) Fluorescence emission spectra of 1 μM POR in the presence and absence of 20 μM NADPH following excitation at 295 nm. (B) Typical stopped-flow fluorescence transient measured over 25 ms and fitted to a single exponential (see Table 1) upon mixing of 1 μM POR and 20 μM NADPH. The inset shows a typical kinetic transient recorded over 100 s, which could be fitted to a double exponential function. An excitation wavelength of 295 nm was used, and the fluorescence emission was measured using a 400 nm cut-off filter. (C) The dependence of the observed rate (k_{obs}) of all three phases of the fluorescence increase on the concentration of NADPH. The error bars were calculated from the average of at least 3 traces. All measurements were recorded at 25 °C as described in the Materials and Methods.

obtained in the FRET experiments (Figure 3A). Although the initial step remains the major component in the overall anisotropy change, the second phase also contributes significantly to the total amplitude; the slower phase contributes only approximately 6 % of the anisotropy signal (Table 1).

Competitive Inhibition of NADPH Binding in Stopped-Flow Studies. To investigate the nature of the interactions formed in the three kinetic phases for NADPH binding we have repeated stopped-flow experiments over a range of 2′5′ ADP and β-nicotinamide monophosphate concentrations. We found that the rate of the initial (fastest) phase of the binding

Table 1: Kinetic and Quasi Thermodynamic Parameters for the Binding of NADPH to POR[a]

kinetic phase	k_{obs} (s^{-1})	% of total signal		$\Delta H^{\ddagger}$ (kJ mol^{-1})	$\Delta S^{\ddagger}$ (J K^{-1} mol^{-1})
		FRET	anisotropy		
first	436.4 ± 53.8	60.6 ± 7.9	66.9 ± 15.1	34.6 ± 3.0	−77.8 ± 6.7
second	1.62 ± 0.43	9.3 ± 0.6	27.1 ± 1.0	81.2 ± 4.4	36.3 ± 2.3
third	0.045 ± 0.004	30.1 ± 1.2	5.9 ± 0.2	67.8 ± 1.4	−5.1 ± 0.2

[a] The rates and relative amplitudes of each step have been measured at 25 °C. The enthalpies of activation, $\Delta H^{\ddagger}$, and the entropies of activation, $\Delta S^{\ddagger}$, have been calculated by fitting the temperature-dependence data to the Eyring equation for each step.

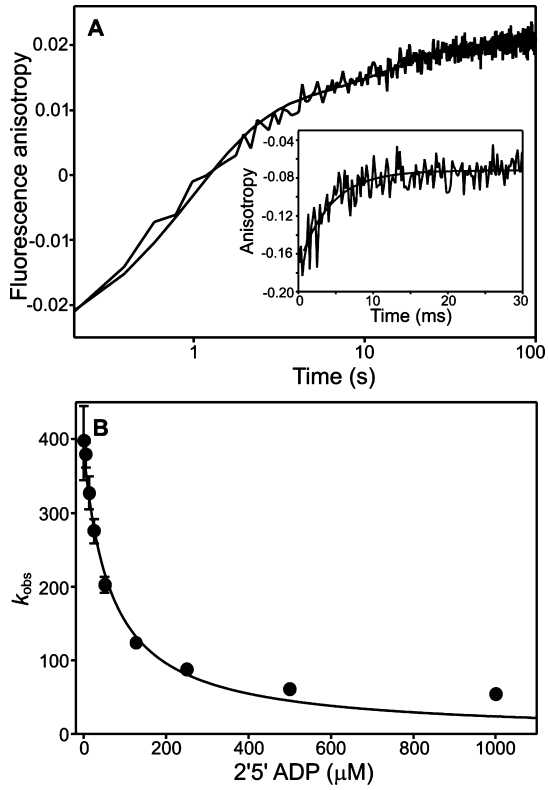

FIGURE 3: The kinetics of NADPH binding probed by fluorescence anisotropy and competitive inhibition studies. (A) Typical stopped-flow fluorescence anisotropy transient measured over 100 s and fitted to a double exponential function upon mixing of 1 μM NADPH and 20 μM POR. The inset shows a typical fluorescence anisotropy transient recorded over 30 ms, which has been fitted to a single exponential. An excitation wavelength of 340 nm was used and the fluorescence anisotropy was measured using a 400 nm cut-off filter as described in the Materials and Methods. (B) The dependence of the observed rate (k_{obs}) of the fast phase of NADPH binding on the concentration of 2′5′ ADP. The error bars were calculated from the average of at least 3 traces. All measurements were recorded at 25 °C as described in the Materials and Methods.

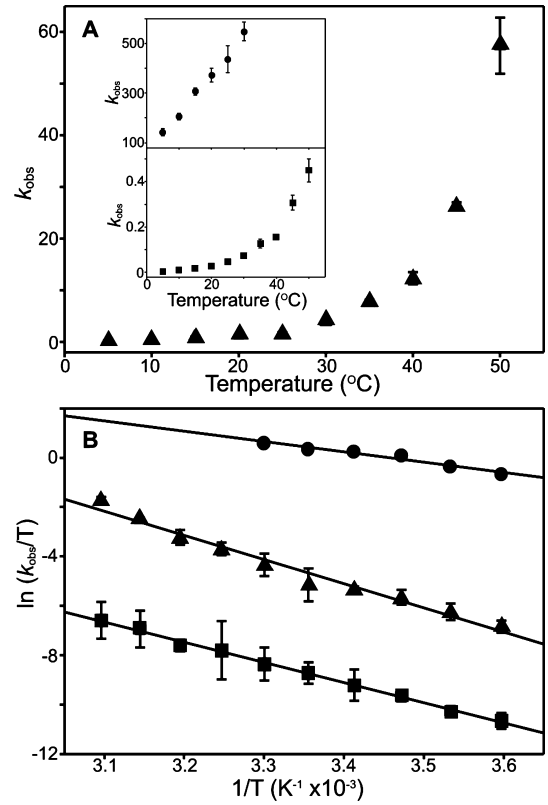

FIGURE 4: Temperature dependence of the kinetics of NADPH binding. (A) The dependence of the observed rates (k_{obs}) of the second phase of NADPH binding on temperature. The inset shows the temperature dependence of the fast and slow phases of NADPH binding. Transients were recorded over a range of temperatures from 5−50 °C and fitted to either a single (fast phase) or a double (slower phases) exponential function. (B) Eyring plot of ln (k_{obs}/T) versus $1/T$ for all three phases of the NADPH binding process. The circles represent the fast phase, the triangles represent the second phase and the squares represent the slow phase. The data were fitted to the Eyring equation, allowing the enthalpy of activation, $\Delta H^{\ddagger}$, and entropy of activation, $\Delta S^{\ddagger}$, to be calculated (Table 1). The error bars were calculated from the average of at least 3 traces.

trace is dependent on the concentration of 2′5′ ADP with a competitive inhibition constant, K_i, calculated to be 3.02 ± 0.29 μM (Figure 3B). In contrast, the presence of β-nicotinamide monophosphate has no effect on the rate of this step (data not shown). Furthermore, various concentrations of 2′5′ ADP (0−1 mM) and β-nicotinamide monophosphate (0−5 mM) were found to have no influence on the rate of the subsequent two steps in the binding process (data not shown).

Temperature-Dependence of Rate Constants for NADPH Binding. The rates of all three kinetic phases observed for NADPH binding were measured over a range of temperatures from 5−50 °C, although it was not possible to measure rate constants for the initial phase above 30 °C as it became too fast to observe in stopped-flow experiments (Figure 4A). To obtain quasi thermodynamic information for NADPH binding, data were analyzed in the form of an Eyring plot of ln (k_{obs}/T) vs $1/T$ (Figure 4B). The enthalpy of activation, $\Delta H^{\ddagger}$, was calculated from the slope of each plot, and the entropy of activation, $\Delta S^{\ddagger}$, was calculated by extrapolation to the ordinate axis for each of the phases (Table 1).

Spectral Changes Associated with Pchlide Binding. Low temperature spectroscopy measurements have previously shown that upon binding to POR, in the presence of either NADPH or $NADP^+$, the absorbance and fluorescence maxima of Pchlide red-shift by several nanometers (*13*). In room temperature measurements this manifests itself by a broadening of the Pchlide absorbance band in the 630−650 nm region (Figure 5A inset). Absorption difference spectra

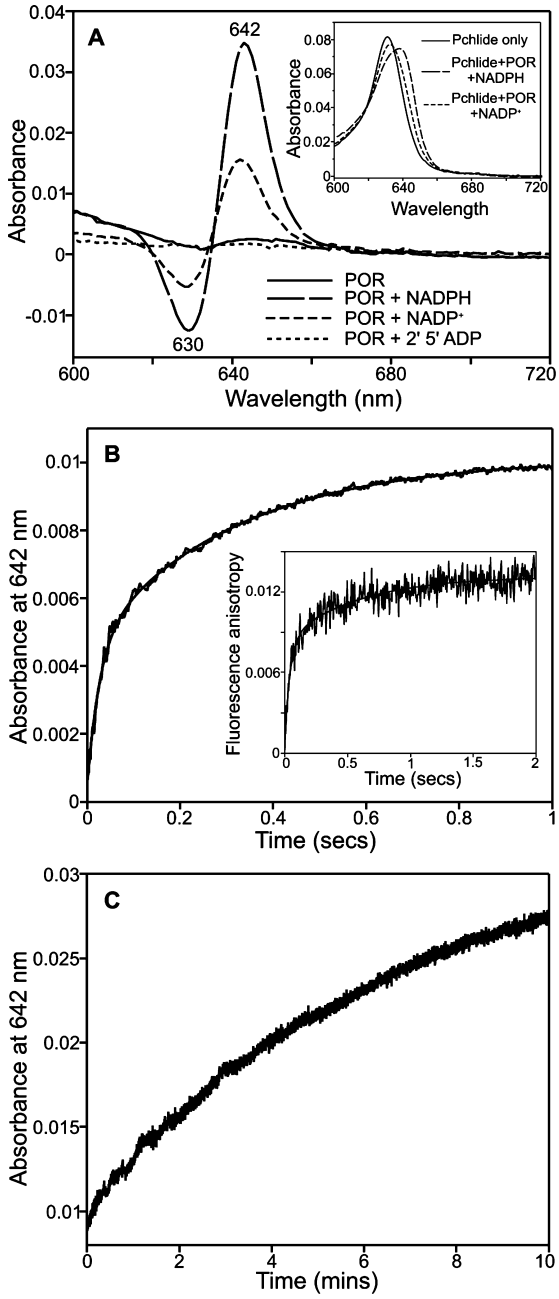

FIGURE 5: Absorbance and kinetic changes associated with Pchlide binding. (A) Absorbance difference spectra of Pchlide (2.35 μM) in the presence of either POR (45 μM), POR + NADPH (250 μM), POR + $NADP^+$ (2 mM) or POR + 2′5′ ADP (2 mM), using a Pchlide only sample as a blank. The inset shows the full absorbance spectra of the various Pchlide species. (B) Typical stopped-flow absorbance transient at 642 nm, measured over 1 s and fitted to a double exponential function (see Table 1), upon mixing of 2.5 μM Pchlide with 30 μM POR and 250 μM NADPH. The inset shows a typical stopped-flow fluorescence anisotropy transient measured over 2 s and fitted to a double exponential function. An excitation wavelength of 450 nm was used and the fluorescence anisotropy was measured using a 595 nm cut-off filter as described in the Materials and Methods. (C) A typical kinetic trace of 2.5 μM Pchlide in the presence of 30 μM POR and 250 μM NADPH, recorded over 10 min in a spectrophotometer, showing the absorbance increase at 642 nm. All measurements were recorded at 25 °C.

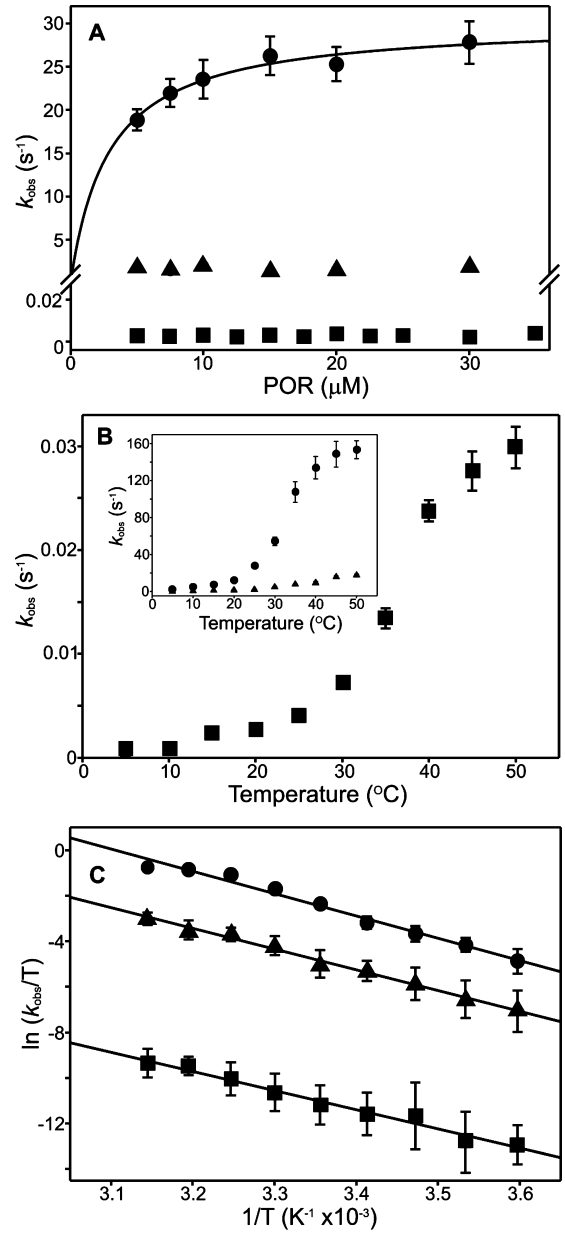

FIGURE 6: Dependence of the kinetics of Pchlide binding on Pchlide concentration and temperature. (A) The dependence of the observed rate (k_{obs}) of all three phases of the absorbance increase at 642 nm on the concentration of Pchlide. The data for the fast phase were fitted to eq 1 (Materials and Methods) to calculate the rate constant and K_d for binding. All measurements were recorded at 25 °C, and the error bars were calculated from the average of at least 3 traces. (B) The dependence of the observed rates (k_{obs}) of the slow phase of Pchlide binding on temperature. The inset shows the temperature dependence of the initial two phases of Pchlide binding. Transients were recorded over a range of temperatures from 5−50 °C and fitted to either a double (faster phases) or a single (slow phase) exponential function. (C) Eyring plot of $\ln(k_{obs}/T)$ versus $1/T$ for all three phases of the Pchlide binding process. The circles represent the fast phase, the triangles represent the second phase and the squares represent the slow phase. The data were fitted to the Eyring equation, allowing the enthalpy of activation, $\Delta H^{\ddagger}$, and entropy of activation, $\Delta S^{\ddagger}$, to be calculated (Table 2). The error bars were calculated from the average of at least 3 traces.

revealed that this broadening is due to a decrease in the 630 nm band associated with "free" Pchlide together with an increase in absorbance at 642 nm attributed to the formation of the ternary complex species (Figure 5A). Absorption spectra also revealed that changes are not observed in the 630−650 nm region when measurements are repeated in the absence of cofactor or in the presence of 2′5′ ADP (Figure 5A).

Table 2: Kinetic and Quasi Thermodynamic Parameters for the Binding of Pchlide to POR[a]

kinetic phase	rate (s^{-1})	% of total amplitude	$\Delta H^{\ddagger}$ (kJ mol^{-1})	$\Delta S^{\ddagger}$ (J K^{-1} mol^{-1})
first	30.2 ± 0.9	12.0 ± 1.9	81.4 ± 4.2	55.3 ± 3.2
second	1.67 ± 0.25	20.6 ± 3.5	75.7 ± 2.3	16.2 ± 0.6
third	$2.05 \pm 0.34 \times 10^{-3}$	67.4 ± 7.2	69.9 ± 4.0	-54.6 ± 5.1

[a] The rates and relative amplitudes of each step have been measured at 25 °C. The enthalpies of activation, $\Delta H^{\ddagger}$, and the entropies of activation, $\Delta S^{\ddagger}$, have been calculated by fitting the temperature-dependence data to the Eyring equation for each step.

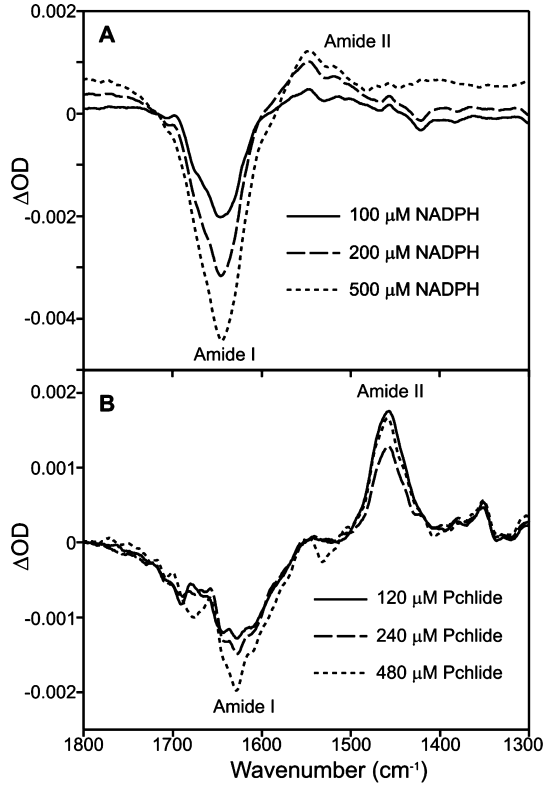

FIGURE 7: Protein conformational changes probed by FTIR spectroscopy. (A) FTIR absorbance difference spectra of POR (270 μM) in the presence of increasing concentrations of NADPH coenzyme, using a POR only sample as a blank. (B) FTIR absorbance difference spectra of POR (270 μM) and NADPH (1 mM) in the presence of increasing concentrations of Pchlide, using a POR−NADPH sample as a blank. The spectral changes in the amide I and amide II regions indicate conformational changes in the enzyme upon binding.

In addition to red-shifts in the absorbance and fluorescence maxima, there is also an increase in fluorescence anisotropy from the Pchlide molecule upon binding to POR in the presence of $NADP^+$. The fluorescence anisotropy at 635 nm increases from approximately 0.025 in the absence of enzyme to approximately 0.16 at 25 μM POR (data not shown). There is no noticeable increase in the anisotropy signal when measurements are repeated in the absence of NADP(H) coenzyme or in the presence of 2′5′ ADP, confirming that Pchlide is only able to bind to POR in the presence of NADP(H).

Rate Constants for Binding of Pchlide Substrate to the POR−NADP$^+$ Complex. We measured the rate of Pchlide binding to the POR−$NADP^+$ complex by measuring both the increase in absorbance at 642 nm and the increase in fluorescence anisotropy from the Pchlide molecule following rapid mixing in a stopped-flow spectrometer. These measurements revealed that binding traces for Pchlide binding comprise an initial biphasic absorbance increase that is accompanied by a simultaneous increase in fluorescence anisotropy (Figure 5B). A much slower third phase, occurring over several minutes, is identified in a standard spectrophotometer by monitoring the increase in absorbance at 642 nm upon binding of Pchlide to a POR−NADPH complex (Figure 5C); a comparable result was also obtained on adding Pchlide to a POR−$NADP^+$ complex.

We measured the observed rate constant for each kinetic phase over a range of Pchlide concentrations. The analysis showed that only the initial (fast) phase exhibits a dependence on the concentration of Pchlide with a calculated K_d of 2.8 $\pm$ 0.4 μM for dissociation of the POR−$NADP^+$−Pchlide complex to the component POR−$NADP^+$ complex and free Pchlide (Figure 6A). The rate constants and relative amplitudes of each phase are summarized in Table 2, which reveal that the majority of the absorbance change at 642 nm is associated with the final step in the binding process.

Temperature-Dependence of Pchlide Binding. As for binding of NADPH to POR, we also measured the rates of all three phases of Pchlide binding to the POR−$NADP^+$ complex over a range of temperatures from 5−50 °C (Figure 6B). Again, quasi thermodynamic information was obtained by fitting data using an Eyring plot of $\ln(k_{obs}/T)$ vs $1/T$ (Figure 6C). The enthalpy of activation, $\Delta H^{\ddagger}$, was calculated from the slope of each plot, and the entropy of activation, $\Delta S^{\ddagger}$, was calculated by extrapolation to the ordinate axis for each of the phases (Table 2).

FTIR Measurements. To probe further the involvement of protein conformational change in substrate binding we measured the absorption spectra of POR in the mid-infrared region in the presence and absence of substrates (Figure 7). The FTIR difference spectra (NADPH-bound minus "free" enzyme) revealed that relatively large changes in the amide I and II regions are observed upon binding of NADPH, consistent with changes in the secondary structure of the enzyme (Figure 7A). In addition, there are further structural changes induced upon binding of the Pchlide substrate, as shown by the FTIR difference spectra (Pchlide−POR−NADPH minus POR−NADPH) in Figure 7B.

DISCUSSION

Owing to its unique dependence on light for activity, it has been shown previously that the chlorophyll biosynthesis enzyme, POR, is an excellent model system for studying aspects of enzyme mechanism (*1*). A series of reaction intermediates have been identified, which has allowed the entire catalytic cycle to be resolved (*11*−*16*). However, despite the fact that it is possible to isolate the ternary enzyme−substrate species in the dark, there is currently a lack of information about the slower substrate binding events leading to its formation, especially in connection with conformational events linked to substrate binding. Consequently, in the present work we have shown that stopped-

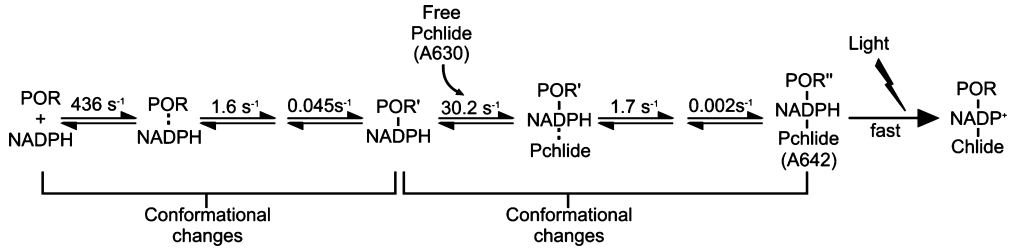

FIGURE 8: Kinetic scheme of the substrate binding events in POR. The calculated rates of all of the binding steps are the sum of the forward and reverse rate constants and provide a detailed kinetic description of these initial steps in the reaction mechanism of POR. The binding of both substrates is controlled by conformational changes in the protein.

flow measurements, when combined with a variety of spectroscopic probes, are excellent vehicles for studying these slower events in the catalytic cycle, prior to the subsequent chemical steps. The binding of each substrate is accompanied by distinct spectroscopic signals, and these have allowed us to study in detail conformational events linked to substrate binding and to propose the more complete kinetic scheme depicted in Figure 8. We emphasize that binding of NADPH to POR alone is not a step within the proposed catalytic cycle of POR (*15, 17*), but the multiple conformational changes observed serve to indicate the complex nature of the binding process (see below for further discussion), which is likely to be a feature of NADPH binding to the catalytically relevant POR−Chlide complex (Figure 1). By contrast, the binding of Pchlide to the POR−NADPH complex is directly relevant to the catalytic cycle, and as with NADPH binding to POR alone, involves a series of complex conformational events.

Our studies reveal that Pchlide can only bind to the coenzyme-bound form of POR and has no apparent affinity for the "free" enzyme. This finding is consistent with previous studies in etioplasts (*24, 25*) and confirms that the initial step in the complete catalytic cycle is the binding of NADPH coenzyme, which then facilitates binding of the Pchlide substrate to form the ternary enzyme−substrate complex. This appears to be common to all members of the SDR superfamily of enzymes, such as the dihydrofolate reductases, where binding of nicotinamide coenzyme precedes binding of the second substrate (*26*−*28*). Similarly, the order of product release also appears to be the same between POR and other members of the SDR family, where release of the coenzyme product occurs prior to the Chlide product (*15, 17*).

We have also shown that the binding of NADPH is itself a complex process, involving at least three distinguishable kinetic phases. The rate constants for these identified kinetic steps do not exhibit a dependence on coenzyme concentration, indicating that they do not represent encounter complex formation. They do show, however, that the binding process is driven by conformational changes in the protein, and this therefore rules out a simple bimolecular mechanism for complex assembly. This is substantiated by our FTIR measurements which, through changes in the amide I and amide II regions of the IR spectrum, confirm that binding of the NADPH is accompanied by structural changes in the enzyme. Such conformational rearrangements are likely to be analogous to the structural changes that have been proposed to occur during the product release steps later in the catalytic cycle (*14, 15, 17*).

The first identified kinetic phase in the NADPH binding process has the largest associated anisotropy signal and is inhibited by ADP, suggesting that it involves an initial anchoring of the ADP moiety of NADPH in the active site. That nicotinamide monophosphate has no apparent influence on any of the kinetic phases suggests that the nicotinamide portion of NADPH binds later and/or is less tightly held by the enzyme, a finding that is similar to the observed bipartite binding of NADPH in diflavin reductase enzymes, such as cytochrome P450 reductase (*29*). The second kinetic phase for NADPH binding to POR is accompanied by a significant anisotropy signal. This suggests that a "locking in" of the nicotinamide portion of the NADPH coenzyme might occur in this kinetic phase, mediated by rearrangements in the protein that are responsible for the correct positioning of the nicotinamide portion of the NADPH molecule. Finally, there are likely to be further small structural changes during the final phase of the binding process as the cofactor is optimally aligned in the enzyme active site prior to light induced hydride transfer from NADPH to Pchlide.

We have also shown that the subsequent binding of the Pchlide substrate is a complicated process involving further conformational changes in the protein. While a relatively fast biphasic reaction with an associated increase in fluorescence anisotropy is likely to represent the formation of an initial complex, slower substrate-induced conformational changes within the enzyme are required for the formation of the final photoactive ternary complex. These slow structural rearrangements appear to be the rate-limiting step in the entire catalytic cycle and are responsible for the red-shift in the Pchlide absorbance maximum, which has previously been suggested to result from interactions with the nicotinamide cofactor (*13*). Combined, the conformational changes identified allow proposal of a more detailed kinetic scheme in which rate limiting conformational changes accompanying substrate and coenzyme binding have been identified (Figure 8).[2]

In summary, we have now used a number of spectroscopic and kinetic probes to study the kinetics and thermodynamics of the rate-limiting substrate binding events in the light-driven enzyme, POR. We have shown that the binding processes are complex, involving a number of different conformational states leading to the formation of the final "poised" photo-

[2] The reported turnover number for thermophilic POR enzyme is ~0.2 s^{-1} at 50 °C (*30*). The observed rate constants (i.e., the sum of the forward and reverse rate constants) for the third, slow conformational changes observed on binding NADPH or Pchlide are lower than the steady-state turnover number. However, it is important to note that these observed rate constants for the conformational changes were measured in the absence of light activation, and at ligand concentrations approximately equal to the dissociation constant for the POR−ligand complex. For this reason, a rigorous comparison of the observed rate constants for the conformational events and the turnover number measured under steady-state turnover conditions is not possible.

active state. As a result, this work presents the first detailed studies on the slow, rate-limiting steps in the POR-catalyzed reaction and provides important information on the formation of a reactive complex that is primed for catalysis.

REFERENCES

1. Heyes, D. J., and Hunter, C. N. (2005) Making light work of enzyme catalysis: protochlorophyllide oxidoreductase. *Trends Biochem. Sci. 30*, 642–649.
2. Lebedev, N., and Timko, M. P. (1998) Protochlorophyllide photoreduction. *Photosynth. Res. 58*, 5–23.
3. Aronsson, H., Sundqvist, C., and Dahlin, C. (2003) POR hits the road: import and assembly of a plastid protein. *Plant Mol. Biol. 51*, 1–7.
4. Jörnvall, H., Persson, B., Krook, M., Atrian, S., Gonzalez-Duarte, R., Jeffery, J., and Ghosh, D. (1995) Short-chain dehydrogenases/reductases (SDR). *Biochemistry 34*, 6003–6013.
5. Oppermann, U., Filling, C., Hult, M., Shafqat, N., Wu, X., Lindh, M., Shafqat, J., Nordling, E., Kallberg, Y., Persson, B., and Jörnvall, H. (2003) Short-chain dehydrogenases/reductases (SDR): the 2002 update. *Chem. Biol. Interact. 143*−*144*, 247–253.
6. Kohen, A., Cannio, R., Bartolucci, S., and Klinman, J. P. (1999) Enzyme dynamics and hydrogen tunnelling in a thermophilic alcohol dehydrogenase. *Nature 399*, 496–499.
7. Boehr, D. D., McElheny, D., Dyson, H. J., and Wright, P. E. (2006) The dynamic energy landscape of dihydrofolate reductase catalysis. *Science 313*, 1638–1642.
8. Valera, V., Fung, M., Wessler, A. N., and Richards, W. R. (1987) Synthesis of 4R- and 4S-tritium labeled NADPH for the determination of the coenzyme stereospecificity of NADPH: protochlorophyllide oxidoreductase. *Biochem. Biophys. Res. Commun. 148*, 515–520.
9. Begley, T. P., and Young, H. (1989) Protochlorophyllide reductase. 1. Determination of the regiochemistry and the stereochemistry of the reduction of protochlorophyllide to chlorophyllide. *J. Am. Chem. Soc. 111*, 3095–3096.
10. Wilks, H. M., and Timko, M. P. (1995) A light-dependent complementation system for analysis of NADPH:protochlorophyllide oxidoreductase. Identification and mutagenesis of two conserved residues that are essential for enzyme activity. *Proc. Natl. Acad. Sci. U.S.A. 92*, 724–728.
11. Lebedev, N., and Timko, M. P. (1999) Protochlorophyllide oxidoreductase B-catalyzed protochlorophyllide photoreduction in vitro: Insight into the mechanism of chlorophyll formation in light-adapted plants. *Proc. Natl. Acad. Sci. U.S.A. 96*, 9954–9959.
12. Lebedev, N., Karginova, O., McIvor, W., and Timko, M. P. (2001) Tyr275 and Lys279 stabilize NADPH within the catalytic site of NADPH:protochlorophyllide oxidoreductase and are involved in the formation of the enzyme photoactive state. *Biochemistry 40*, 12562–12574.
13. Heyes, D. J., Ruban, A. V., Wilks, H. M., and Hunter, C. N. (2002) Enzymology below 200 K: the kinetics and thermodynamics of the photochemistry catalyzed by protochlorophyllide oxidoreductase. *Proc. Natl. Acad. Sci. U.S.A. 99*, 11145–11150.
14. Heyes, D. J., Ruban, A. V., and Hunter, C. N. (2003) Protochlorophyllide oxidoreductase: "Dark" reactions of a light-driven enzyme. *Biochemistry 42*, 523–528.
15. Heyes, D. J., and Hunter, C. N. (2004) Identification and characterization of the product release steps within the catalytic cycle of protochlorophyllide oxidoreductase. *Biochemistry 43*, 8265–8271.
16. Heyes, D. J., Heathcote, P., Rigby, S. E. J., Palacios, M. A., van.Grondelle, R., and Hunter, C. N. (2006) The first catalytic step of the light-driven enzyme protochlorophyllide oxidoreductase proceeds via a charge transfer complex. *J. Biol. Chem. 281*, 26847–26853.
17. Heyes, D. J., Sakuma, M., and Scrutton, N. S. (2007) Laser excitation studies of the product release steps in the catalytic cycle of the light-driven enzyme, protochlorophyllide oxidoreductase. *J. Biol. Chem. 282*, 32015–32020.
18. Heyes, D. J., Hunter, C. N., van.Stokkum, I. H. M., van Grondelle, R., and Groot, M. L. (2003) Ultrafast enzymatic reaction dynamics in protochlorophyllide oxidoreductase. *Nat. Struct. Biol. 10*, 491–492.
19. Dietzek, B., Kiefer, W., Hermann, G., Popp, J., and Schmitt, M. (2006) Solvent effects on the excited-state processes of protochlorophyllide: a femtosecond time-resolved absorption study. *J. Phys. Chem. B 110*, 4399–4406.
20. Dietzek, B., et al. (2006) The excited-state chemistry of protochlorophyllide a: a time-resolved fluorescence study. *Chem. Phys. Chem 7*, 1727–1733.
21. Zhao, G. J., and Han, K. L. (2008) Site-specific solvation of the photoexcited protochlorophyllide a in methanol: formation of the hydrogen-bonded intermediate state induced by hydrogen-bond strengthening. *Biophys. J. 94*, 38–46.
22. Sytina, O., Heyes, D. J., Hunter, C. N., Alexandre, M. T., van Stokkum, I. H. M., van Grondelle, R., and Groot, M. L. (2008) Conformational changes in an ultrafast light-driven enzyme determine catalytic activity. *Nature* (in press).
23. Li, B., and Lin, S. X. (1996) Fluorescence-energy transfer in human estradiol 17 beta-dehydrogenase-NADPH complex and studies on the coenzyme binding. *Eur. J. Biochem. 235*, 180–186.
24. Boddi, B., Ryberg, M., and Sundqvist, C. (1992) The formation of a short-wavelength chlorophyllide form at partial phototransformation of protochlorophyllide in etioplast inner membranes. *J. Photochem. Photobiol., B: Biol. 12*, 389–401.
25. Boddi, B., Ryberg, M., and Sundqvist, C. (1993) Analysis of the 77 K fluorescence emission and excitation-spectra of isolated etioplast inner membranes. *J. Photochem. Photobiol., B: Biol 21*, 125–133.
26. Fierke, C. A., Johnson, K. A., and Benkovic, S. J. (1987) Construction and evaluation of the kinetic scheme associated with dihydrofolate reductase from *Escherichia coli*. *Biochemistry 26*, 4085–4092.
27. Cameron, C. E., and Benkovic, S. J. (1997) Evidence for a functional role of the dynamics of glycine-121 of *Escherichia coli* dihydrofolate reductase obtained from kinetic analysis of a site-directed mutant. *Biochemistry 36*, 15792–15800.
28. Schnell, J. R., Dyson, H. J., and Wright, P. E. (2004) Structure, dynamics, and catalytic function of dihydrofolate reductase. *Annu. Rev. Biophys. Biomol. Struct. 33*, 119–140.
29. Döhr, O., Paine, M. J., Friedberg, T., Roberts, G. C., and Wolf, C. R. (2001) Engineering of a functional human NADH-dependent cytochrome P450 system. *Proc. Natl. Acad. Sci. U.S.A. 98*, 81–86.
30. McFarlane, M. J., Hunter, C. N., and Heyes, D. J. (2005) Kinetic characterisation of the light-driven protochlorophyllide oxidoreductase (POR) from *Thermosynechococcus elongatus*. *Photochem. Photobiol. Sci. 4*, 1055–1059.

BI801521C